JOURNAL OF AIRCRAFT
Vol. 31, No. 1, Jan.–Feb. 1994

Sonic Boom of the Oblique Flying Wing

A. Van der Velden*
Deutsche Airbus GmbH, D-2800 Bremen 1, Germany
and
I. Kroo†
Stanford University, Stanford, California 94305

This article presents an analysis of oblique flying wing sonic boom characteristics. This long asymmetric wing provides a reduction in sonic boom loudness as well as aerodynamic and structural improvements over conventional transports. The wing is represented by an oblique line equivalent area distribution, a panel model, and a high-definition surface model. The near-field pressure signature of the first two representations is found using the Whitham *F*-function method applied to the oblique equivalent area distribution and the panel model. The near-field pressure distribution of the high-definition surface model was found using TranAir, a full-potential analysis code. Good agreement between the methods was found. The near-field signature is extrapolated through the standard atmosphere by the Thomas waveform parameter method. The asymmetry in the geometry leads to an asymmetrical sonic boom under the flight track. The bow shock amplitude is typically between 50–75 N/m² depending on the size, weight, and altitude of the configuration. The aft shock has only one-half the amplitude of the bow shock due to favorable volume-lift interference. This article also includes a simple method to estimate the maximum sonic boom overpressures of oblique flying wings.

Nomenclature

A = area
A_e = equivalent area
A_v = equivalent area due to volume
a = speed of sound
a_{ax} = semiminor axis of flat elliptic oblique wing
b_{ax} = semimajor axis of flat elliptic oblique wing
f = frequency
h = altitude
l = length of pressure signal
ℓ = lift per unit length
M = Mach number
p = pressure
r = radial distance from X axis to near field
t = dimensionless expressions of the x coordinate, Eq. (10)
W = aircraft weight
x = dimensionless expressions of the x coordinate, Eq. (8)
β = Prandtl's compressibility coefficient $\sqrt{M^2 - 1}$
γ = ratio of specific heats
θ = azimuth angle
Λ = sweep angle
τ = dimensionless expression of the x coordinate, Eq. (8)
ω = radian frequency, $2\pi f$

Introduction

IN 1961 Lee[1] proposed an oblique flying wing configuration as an alternative to the delta wing configuration. Unsolved control and aerodynamic problems prevented the further development of the concept. Since 1987 the concept has been reintroduced by Refs. 2–6. The long asymmetric flying wing provides not only aerodynamic and structural improvements over conventional transports, but also a reduction in sonic boom overpressures.

The sonic boom of an oblique wing configuration was investigated experimentally by Hicks and Mendoza.[7] This configuration had a fuselage and was designed for Mach 1.2 flight. They concluded that the sonic boom level of the oblique wing configuration was lower than that of a similar, symmetrical swept wing configuration at the design cruise lift. However, the small sonic boom signature of the isolated oblique wing was overshadowed by the substantial signature of the fuselage. In addition, these wind-tunnel results only dealt with the signature directly under the flight track. In the conceptual design of the oblique flying wing (OFW)[3] a bow-shock amplitude of 67 N/m² was predicted, significantly less than that of the currently proposed high-speed civil transports (HSCTs). This fact, and the current interest in the environmental impact of supersonic flight, motivated the present effort to investigate the sonic boom of an oblique flying wing.

Obique Flying Wing Geometry

The oblique flying wing geometry is represented by three models:

1) An oblique line equivalent area distribution was used to investigate the sonic boom of oblique flying wings as a function of Mach number, sweep, volume, and lift. The line equivalent area distribution represents an elliptically loaded oblique flying wing with a Sears-Haack[8] area distribution. This wing has the minimum induced drag and the minimum wave drag for a configuration of given volume and span in supersonic flow. The line geometry is useful not only because it produces quantitive data of comparable quality to those generated by the more detailed surface models at a fraction of the computational cost, but also because it allows us to explain the results analytically.

2) OFW-5 is an 800-panel linear potential flow model. This model was designed with the method of Ref. 5 to cruise at Mach 1.6. The sonic boom was analyzed for the trimmed start cruise condition. Figure 1 shows a transport derived from this panel geometry. The OFW-5 was only one of many designs completed. The optimum OFW geometry will depend on payload, Mach number, and range as described in Ref. 6. Descriptions of the panel code and the wing geometries are given in Ref. 3.

Received Feb. 20, 1991; revision received Sept. 28, 1992; accepted for publication Oct. 2, 1992.

*Aerospace Specialist, Hünefeldstrasse 1-5, P.O. Box 107845. Member AIAA.
†Associate Professor, Department of Aero Astro. Member AIAA.

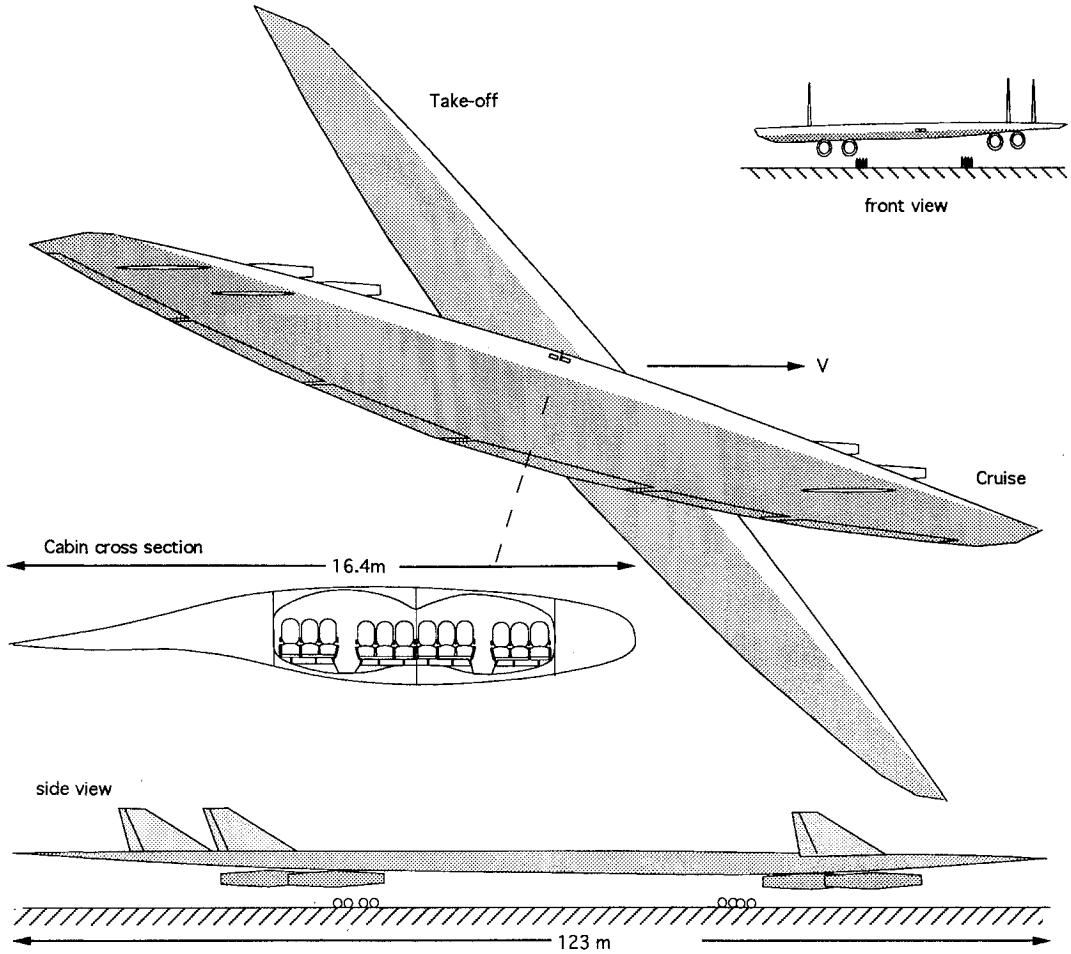

Fig. 1 Mach 1.6 OFW transport.

3) A high-definition surface geometry (13,770 surface points) for the TranAir full potential code was derived from the panel model of the OFW-5. This model also had four flow-through nacelles to study the effects of powerplant-wing interference on sonic boom and drag. The calculations were done independently by Chris Lee at NASA Ames. The vertical fins did not influence the ground signature and were omitted.

The differences in computational cost are very important aspects. To analyze the sonic boom of a line area distribution at one operating condition takes a few seconds on a Macintosh computer. To analyze the panel geometry (excluding 1–2 days for the design) takes a few minutes on a VAX, and it takes 2 h on a CRAY to analyze the high-definition surface geometry.

Near-Field Pressure Distribution

In this section we will first describe the derivation of the sonic boom signature using classic linear theory and the geometric simplifications described in the previous section. Results of this simplified analysis are compared to the results from the panel method and the TranAir full potential method for the OFW-5 model. Figure 2 qualitatively shows the pressure disturbances caused by an oblique flying wing.

The length of the pressure signal at a radial distance r from the flight-axis of the airplane can be determined by examining the intersection of the characteristics with a cylindrical surface at this radial distance. This analysis shows that the length of the signal depends on θ. Figure 2 also defines the left, top, and bottom sides of the signal. The signal length on the left side ($\theta = 0$) is much shorter than the signal length on the right side ($\theta = 180$ deg). This will result in a significant asymmetry in the duration and magnitude of its sonic boom in the near field and even in the far field. For observers more than two lengths away from the aircraft, the OFW can be modeled as an oblique lift and area distribution. For each azimuth angle these distributions are represented by an equivalent body.[9] Figure 3 shows the area distribution corresponding to a given azimuth angle.

Whitham's method[10] can be used to convert the second derivative with respect to length of these area distributions into near-field pressure distributions. The Sears-Haack[8] area distribution with fixed volume can be expressed as

$$A_{\text{volume}}(-1 \le x \le 1) = A_{\max}(1 - x^2)^{1.5} \tag{1}$$

where $A_{\max}$ is the maximum cross-sectional area normal to the oblique line. The x coordinate is centered around the maximum cross-sectional area and is nondimensionalized with twice the area distribution length. The second derivative of the area distribution with respect to length can be expressed as

$$A''_{\text{volume}} = A_{\max}\left[\frac{3x^2}{\sqrt{(1 - x^2)}} - 3\sqrt{(1 - x^2)}\right] \tag{2}$$

Reference 11 gives an expression for the equivalent area distribution due to lift

$$A_{\text{lift}} = \frac{\beta}{\rho U^2}\int_{-1}^{x} \ell(\bar{x}, \theta)\, d\bar{x} \tag{3}$$

ℓ refers to the component of the resultant force per unit length in the oblique plane θ projected on a plane normal to the freestream. For an elliptic lift distribution with a total lift L, this is expressed as

$$\ell(x, \theta) = (2/\pi)L\sqrt{1 - x^2}\sin\theta \tag{4}$$

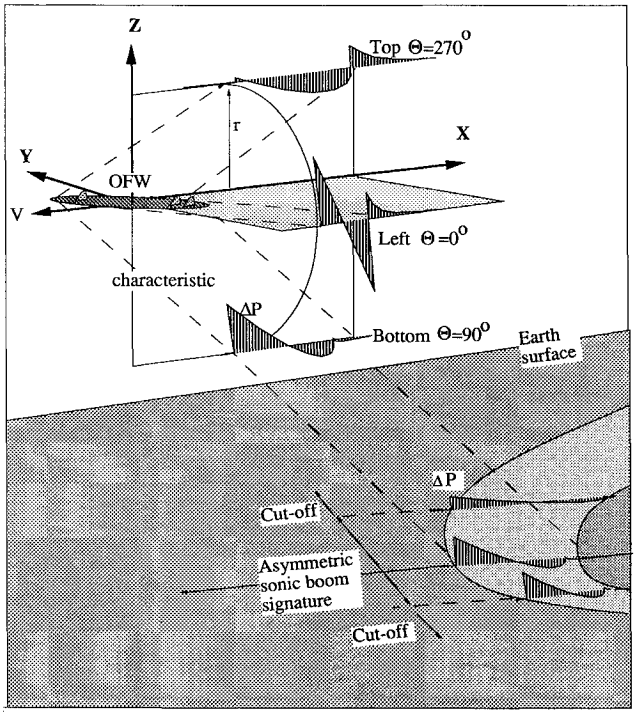

Fig. 2 Pressure disturbances caused by an OFW.

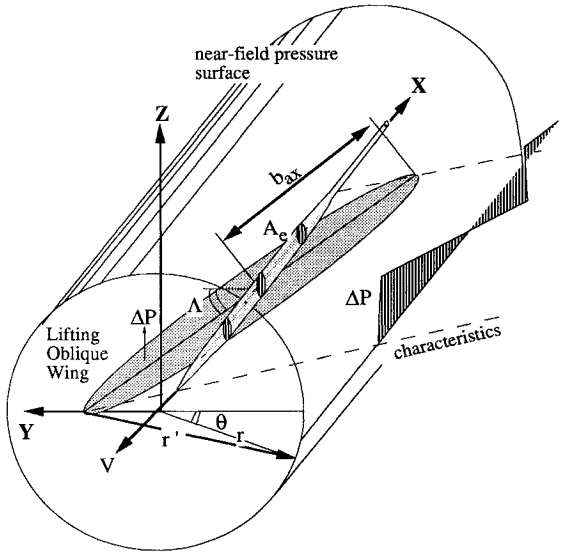

Fig. 3 Slewed equivalent area distribution corresponding to azimuth angle θ.

Substitution in Eq. (3), and replacement of the total lift by W, gives

$$A_{\text{lift}} = \frac{1}{\pi}\left(x\sqrt{1-x^2} + \arcsin x + \frac{\pi}{2}\right)\frac{\beta W}{\rho U^2}\sin\theta \tag{5}$$

The second derivative of the equivalent area distribution due to lift varies as

$$A''_{\text{lift}} = \left[\frac{-2x + 2x^3}{\pi(1-x^2)^{3/2}}\right]\frac{\beta W}{\rho U^2}\sin\theta \tag{6}$$

Figure 4 shows the equivalent area distribution of the oblique flying wing for $\theta = 90$ deg and Mach 1.6.

The total second derivative of the area distribution is the sum of the lift and volume components corrected for the

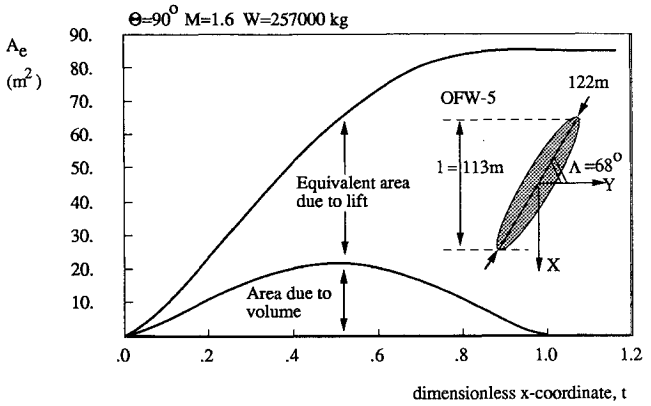

Fig. 4 Equivalent area distribution.

transformation in the x domain from x to t

$$A''_e(t) = 4[A''_{\text{lift}}(t) + A''_{\text{volume}}(t)] \tag{7}$$

where

$$t = [(x + 1)/2] \tag{8}$$

For symmetric configurations, the length of the signal is approximately constant, but for the OFW the length of the signal varies strongly with azimuth angle as shown in Fig. 2. The variation of the length of the signal l with azimuth angle and sweep angle can be expressed as

$$l = 2b_{\text{ax}}(\sin\Lambda - \beta\cos\Lambda\cos\theta) \tag{9}$$

In this expression, b_{ax} represents the semimajor axis of the oblique wing. To calculate the near-field pressure distribution, we use Whitham's method[10]:

$$F(\tau) = \frac{1}{l^{1.5}}\int_0^\tau \frac{A''_e}{2\pi\sqrt{(\tau - t)}}\,dt \quad \text{and} \quad 0 \le \tau \le 1 \tag{10}$$

In this expression τ refers to the nondimensional x location of the pressure signal. This function can be integrated numerically by representing the A''_e distribution as a series of pulses as described in Ref. 12. For each pulse of duration starting at time $t = a$, and ending at time $t = b$, the integral may be written as

$$\int_a^b \frac{A''_e\left(\frac{a+b}{2}\right)}{2\pi\sqrt{(\tau - t)}}\,dt = \frac{A''_e\left(\frac{a+b}{2}\right)}{\pi}\left(\sqrt{\tau - a} - \sqrt{\tau - b}\right) \tag{11}$$

There is also some distortion in the wave shape due to variation of the speed of sound with pressure. This is included by correcting the value of τ corresponding to a pressure disturbance[13]:

$$\tau_{\text{corr}} = \tau - \frac{\sqrt{r}(\gamma + 1)M^4}{\sqrt{2}\beta^{1.5}}F \tag{12}$$

The F function can be converted into a pressure distribution for every observer by multiplication by a constant:

$$\frac{\Delta P}{P} = \frac{\gamma M^2}{\sqrt{2\beta r}}F \tag{13}$$

The obliqueness of the singularity distribution will generate additional errors in the calculation of the pressures and ad-

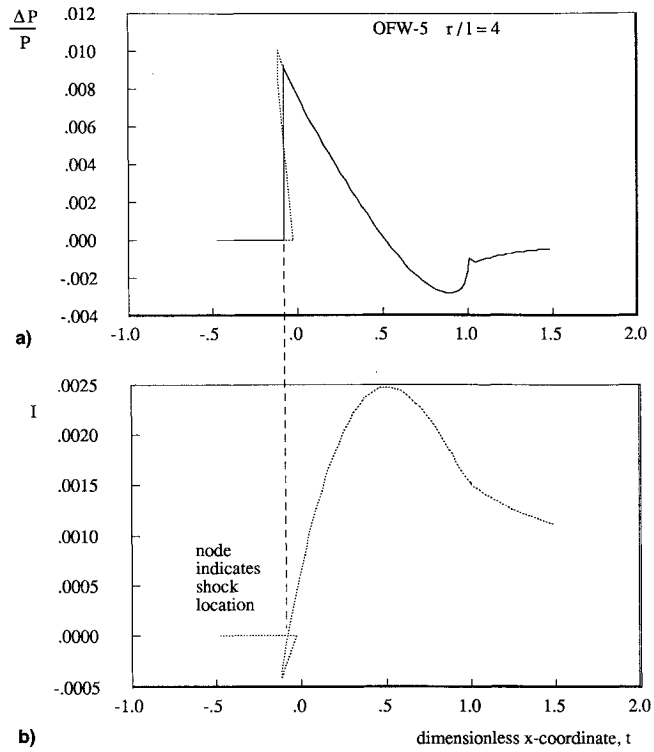

Fig. 5 Near-field pressure signature: a) - - - corrected F-function and b) —— area balanced signature.

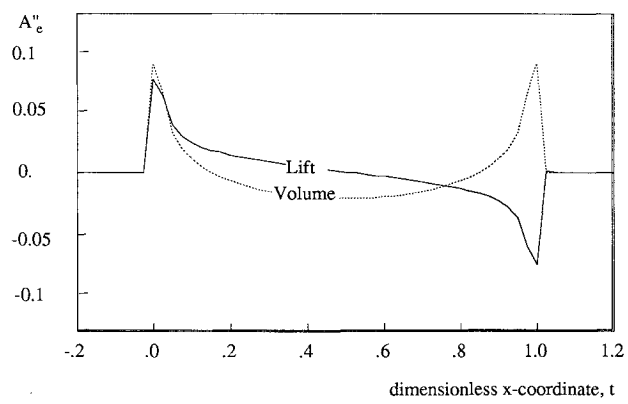

Fig. 6 Cancellation of the aft-shock due to favorable volume-lift interference.

vance time compared with calculations for axisymmetric bodies. These errors are related to r'/r defined in Fig. 3, where

$$r'(\tau) = \sqrt{\{r\cos\theta - [(2\tau - 1)b_{ax}\cos\Lambda]\}^2 + (r\sin\theta)^2} \tag{14}$$

For the signature three lengths away on the left side of the oblique wing, the bow-shock overpressure may be overestimated by 5%, and the advance time correction may be underestimated by 5%. Since the error decreases with increasing radial distance, the *F*-function method is still appropriate for oblique wing far-field calculations.

In most cases the corrected signal represents a physically impossible situation, because we have more than one value for the pressure at a given location. When this occurs a shock will form. The location of the shock can be determined with the area-balancing technique.[14] This method integrates the pressure signal to find the shock location:

$$I = \int_0^{\tau_{corr}} \frac{\Delta P}{P}(\theta, t_{corr})\, dt \tag{15}$$

The shock occurs when the value of the integrated pressure signal plotted against the corrected time crosses itself. This corresponds to a condition where the opposing cutoff areas of the corrected pressure distribution are equal.

Figure 5a shows the corrected near-field pressure signature and the area-balanced pressure signature with shocks at a radial distance of twice the X component of the length of the aircraft. The location of the shocks follows from the integration of the corrected signature as indicated in Fig. 5b. As shown in Fig. 5a, the aft-shock amplitude is much smaller than the bow-shock amplitude. Figure 6 shows the second derivatives of the equivalent area distributions due to lift and volume. The aft-shock pressure is reduced here because the absolute value sum of the second derivatives is less than the absolute value of its components directly upstream from the aft-shock.

A more refined representation of the OFW-5 was created using the panel surface model described in the previous section. The equivalent area distribution of the panel geometry was determined.[9] Once the equivalent area distribution was known, the pressure distribution was obtained in the same way as described for the equivalent area line distribution. The near-field pressures were also obtained directly from TranAir for the high-definition OFW-5.

Ground Signature

The near-field pressure signature will resemble a N-shaped wave more as it propagates away from the aircraft, because disturbances propagate down at the local speed of sound plus the local convective speed, not at the ambient speed of sound. The high-pressure disturbances therefore travel faster, while the low-pressure disturbances will travel slower. The program CLNET[15] calculates the propagation of the wave through the standard atmosphere for a given near-field sonic signature. This program, based on the waveform parameter method, is more suitable for computer application because the necessity of the area-balancing technique is eliminated. Just as with the *F*-function method, the waveform parameter method relies on geometric acoustics for the amplitude and isentropic wave theory for the waveform distortion. Unlike the *F*-function method, which uses the wave age to distort the pressure signature, the waveform parameter method uses a set of parameters and their rate of change to describe the waveform as a function of time. Assuming a reflection factor of 1.9, Fig. 7 shows the ground pressures for the OFW-5 for the line singularity, panel singularity, and TranAir calculations. In view of the high similarity of the signatures, the use of the simpler models is justified. The aft-shock cancellation predicted for the panel model is not as smooth as that of the idealized geometry because the aft-body geometry does not follow the Sears-Haack[8] distribution exactly. The TranAir results are smoother due to grid-coarseness and numerical dissipation. The nacelles have only a very small influence on the ground signature because the inlet and exit stream tube areas are nearly identical.

However, not all near-field pressure disturbances reach the ground. As shown by Kane and Palmer,[16] some acoustic rays

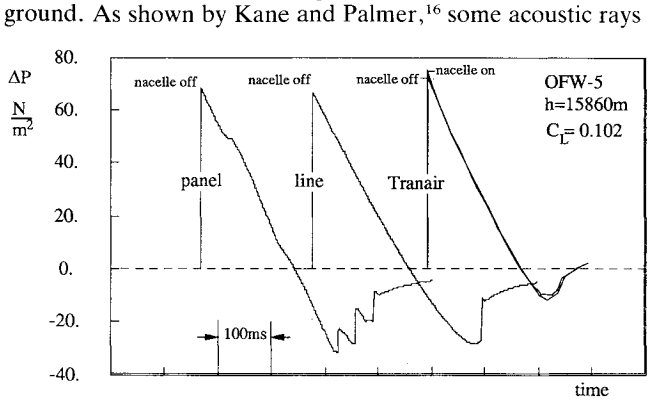

Fig. 7 Ground pressures according to different methods.

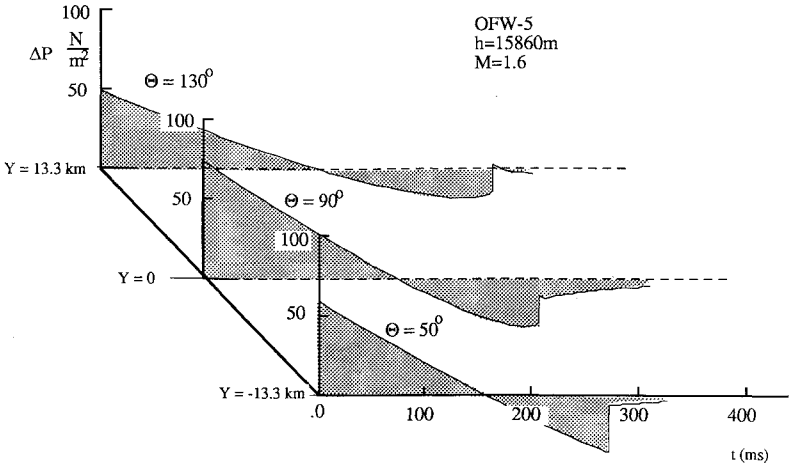

Fig. 8 Lateral distribution of OFW-5 sonic boom overpressures.

are reflected and never reach the ground due to stratified variations in the speed of sound. In the 1962 *U.S. Standard Atmosphere* this occurs when the lateral extent of the sonic boom reaches the cutoff value:

$$(y/h)_{\text{cutoff}} = \sqrt{1 - (a_{\max}/V)^2}[1.74 + 2.01(h_{\text{tp}}/h)] \quad (16)$$

In this expression h_{tp} stands for the tropopause altitude (36,000 ft). The lateral extent of the sonic boom on the Earth's surface is directly influenced by aircraft altitude, speed, and the highest temperature the acoustic ray encounters on its way down. Figure 8 shows the lateral sonic boom signature of the OFW-5. The maximum overpressure is offset from the ground track.

Carlson[12] presented a simplified method for the estimation of the sonic boom of various configurations:

$$\Delta P = [1.9\beta^{0.25}K_s K_a \sqrt{P_h P_g}/(h/l)^{0.75}] \quad (17)$$

In this expression P_h is the pressure at altitude and P_g is the pressure at the ground. A value of 1.12 is reasonable for the atmospheric factor K_a for cruising altitudes between 15–20 km and Mach number between 1.5–2.5. The shape factor K_s of Fig. 9 can now be used to obtain a first approximation to the maximum amplitude of the sonic boom overpressure of an aerodynamically optimized oblique flying wing. K_L is defined as

$$K_L = (\beta C_L S/2l^2) \quad (18)$$

For example, the OFW-5 at the conditions of Fig. 7 has a maximum amplitude of 65 N/m^2 according to the simplified analysis, which is very close to the value predicted by the more involved methods. This method was also applied to the OFWs that were designed for other missions. As shown in Fig. 10, these transports have sonic booms that are substantially lower than those of comparable supersonic transports.

Loudness Analysis and Atmospheric Effects

The infinitely short rise time in ground signatures predicted by these quasilinear methods do not occur in reality. Short rise times require an energy level in the higher frequencies, but the atmosphere attenuates high-frequency pressure disturbances. Figure 11 shows the rise times recorded during operation "yellow hammer" in the 1960s.[17] The range of overpressures was similar to those predicted for the OFW. Typical values for the rise time are between 2–12 ms, depending on the atmospheric conditions and lateral location. Atmospheric influence such as temperature inversion and wind also produce variations in the sonic boom maximum amplitude. Figure 12 also shows the ratio of the maximum sonic boom over-

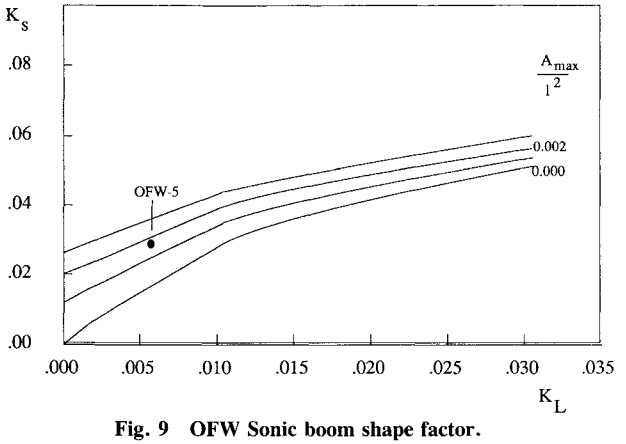

Fig. 9 OFW Sonic boom shape factor.

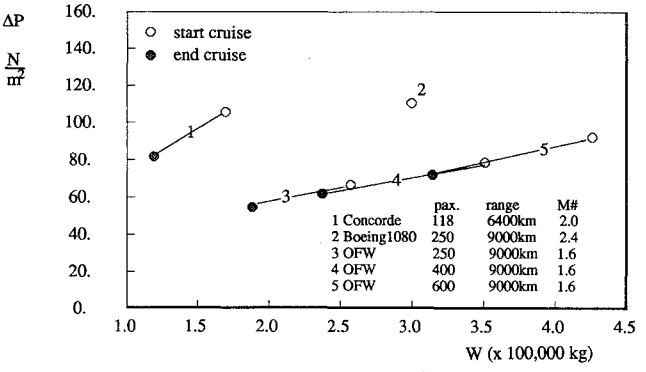

Fig. 10 Range of sonic boom overpressures for various transports as a function of weight.

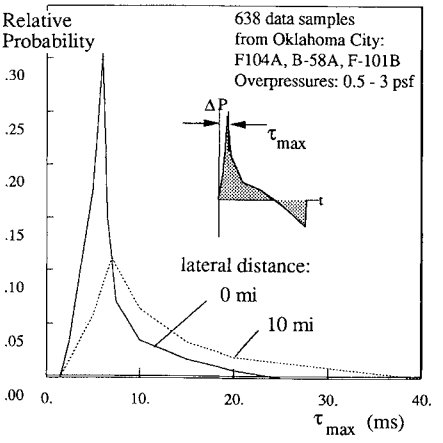

Fig. 11 Relative probability of atmospheric rise-times.

pressures that were predicted with the *F*-function method vs the measured overpressures for these tests. The atmospheric absorption of the higher frequencies is included by sampling the reflected signal with the rise-time. To calculate the loudness of the sonic boom signal, occurring in the time interval t_1 to t_2, this signal is transformed into its frequency domain:

$$F(\omega) = \int_{t_1}^{t_2} P(t)e^{i\omega t}\,dt \tag{19}$$

Following Papoulis[18] we can linearly interpolate between the discrete pressures representing the signal and compute the Fourier transform by a sum of exponentials with time-shifting:

$$F(\omega) \simeq \frac{-1}{\omega^2}\sum_{i=a}^{b} k_i e^{i\omega t} \tag{20}$$

$$k_i = \frac{(p_{i+1} - p_i)}{(t_{i+1} - t_i)} - \frac{(p_i - p_{i-1})}{(t_i - t_{i-1})} \tag{21}$$

$$e^{i\omega t} = \cos(\omega t_i) - i\sin(\omega t_i) \tag{22}$$

The variable k_i is the change in the pressure gradient at sampling point i. The loudness is produced by these gradient jumps. The highest acoustic energy radiated to an observer during the reference time can be calculated by integrating over the interval that contains the largest changes in pressure gradients. Under the flight track of a lifting configuration, this will almost always include the bow shock. The energy in each third octave frequency band "b" can be calculated as follows:

$$E_b = \frac{1}{\pi}\int_{\omega_1}^{\omega_2} |F(\omega)|\,d\omega \tag{23}$$

The weighted sound pressure level (SPL) for each third octave band can be expressed as

$$\mathrm{SPL}_{b,w} = 10\log\left(\frac{E_b}{p_{\mathrm{ref}}^2 t_{\mathrm{ref}}}\right) + \mathrm{SPL}_w \tag{24}$$

The reference sound pressure level is taken to be 20 μN/m^2. The reference time was taken as 1 s. Conforming with a current practice, the *A* weighting was used to get the weighted SPL. Figure 13 shows the sonic boom spectral density and the third octave band *A*-weighted sound pressure levels.

According to Ref. 19, unrestricted flight may be possible for the loudness generated by a 24 N/m^2 N-shaped wave with a 10-ms rise-time, this corresponds to a loudness of 64 dBA with the reference SPL and reference time. A 72 N/m^2 N-shaped wave with a 10-ms rise-time was still considered acceptable by about two-thirds of the population. This level corresponding to 72 dBA was selected by Ref. 19 as the upper limit for flight through restricted corridors.

Figure 14 shows the OFW loudness when we take into account the probable atmospheric variation of rise-time and amplitude. This figure also shows the 65-dBA upper limit to unrestricted flight and a proposed 72-dBA upper limit to flight within restricted corridors.

From this graph it is clear that it is not possible to meet the flight through restricted corridor criterion for most atmospheric conditions. This figure also illustrates the enor-

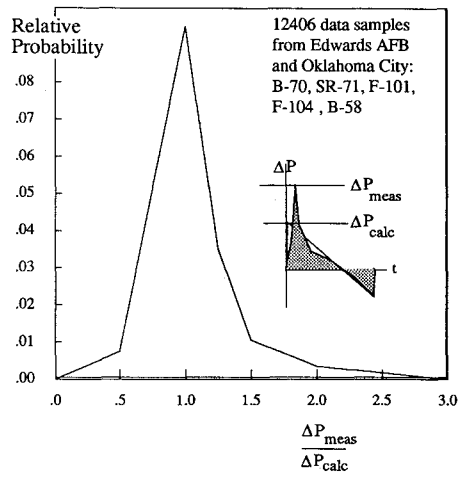

Fig. 12 Relative probability of bow shock amplitudes.

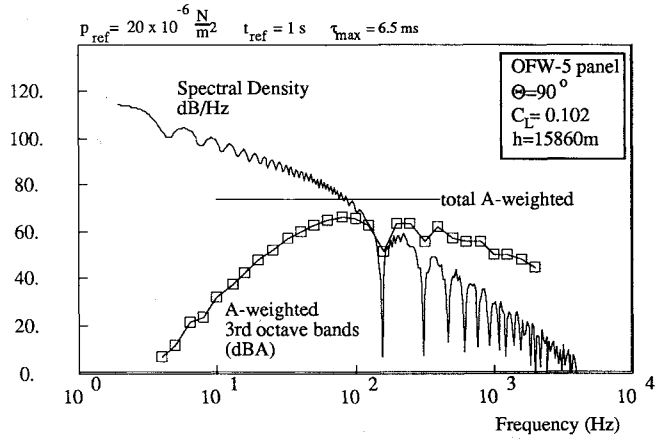

Fig. 13 Sonic boom energy spectral density and loudness evaluation.

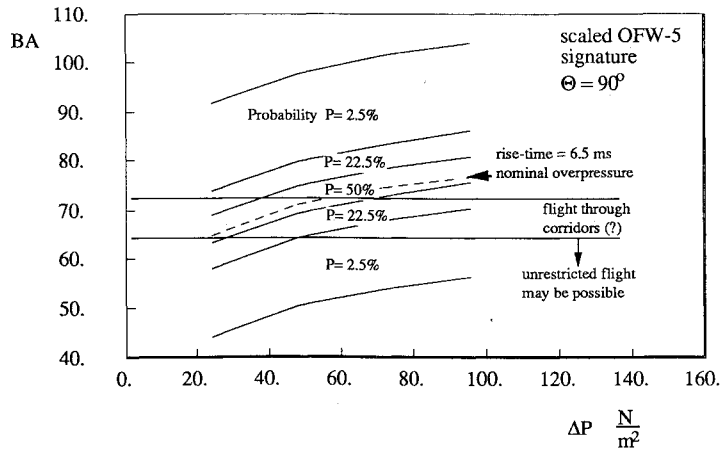

Fig. 14 Oblique flying wing loudness as a function of maximum overpressure.

Table 1 Start cruise total operational loudness comparison

Configuration	Signal	Passengers	Total operational
Concorde	78 dBA	128	0 dBA
HSCT B1080	79 dBA	247	−5 dBA
HSCT B1080 Low boom	77 dBA	268	−7 dBA
OFW250	74 dBA	250	−10 dBA
OFW400	75 dBA	400	−13 dBA
OFW600	76 dBA	600	−15 dBA

mous range of sonic boom loudness due to atmospheric variations. Kane and Palmer[16] reported an estimated 26-dB loudness difference for a single F104 sonic boom. This loudness difference occurred between two microphones only 600 ft from each other along the same flight path and was caused by local atmospheric turbulence.

Loudness Reduction

The baseline oblique flying wing produces lower sonic boom overpressures, but it still produces an unacceptable sonic boom for unrestricted flight. Compared to other designs,[19,20] the greatest advantage comes from the fact that this aircraft has up to twice the payload as current HSCT designs and four times the payload of Concorde. For a given market this will result in fewer flights, and thus less nuisance. Von Gierke and Nixon[21] propose a weighting of 3 dB of every doubling of the number of occurrences. This weighting was substantiated by the Oklahoma City tests. Assuming the same market for all the aircraft considered, each doubling of the payload will therefore result in an effective 3-dB noise reduction. Table 1 compares the signal and total operational loudness of various delta wing and OFW configurations. All signals are compared at start cruise with a 6.5-ms rise-time, and all aircraft have a standard triclass layout.

Even though the aircraft with the greater payloads have slightly higher nominal signal loudnesses, the total operational loudness drops significantly with size. The best OFW would therefore be the 600-passenger version.

The sonic boom can be eliminated completely by flying between Mach 0.9–1.3, depending on atmospheric conditions.[16] The variable geometry oblique flying wing can cruise with the same fuel efficiency as a B747 at these transonic speeds, so this will not result in an additional fuel penalty.

To lower the sonic boom loudness we can also consider changing the geometry. It is not efficient to reduce the sonic boom overpressures by increasing the length. Reducing the sonic boom overpressures from 72 to 48 N/m^2 would require increasing the length of the configuration by 50%, without increasing the weight. This does not seem possible.

It is possible to reduce the loudness by about 2 dB by adding thickness near the nose of the aircraft. This approach was briefly discussed in Ref. 22. Sonic boom minimization techniques do not only increase the drag, but in the case of the OFW they also interfere with the control of the configuration. Addition of thickness to one wing tip results in additional yawing moments. In addition, the large atmospheric loudness variations make this effort almost futile.

Conclusions

The sonic boom of an oblique flying wing modeled with various levels of detail was determined using the "classic" corrected Whitham *F*-function method and TranAir. The following results were obtained:

1) Bow shock overpressure is in the range of 50–90 N/m^2, depending on the geometry and weight and altitude of the configuration, typically one-third less than comparable symmetric configurations.

2) The aft-shock is cancelled due to favorable volume-lift interference.

3) The lateral distribution of the sonic boom signature is distinctively asymmetric.

4) Nacelles configured for Mach 1.6 do not significantly increase the bow shock overpressure.

5) The sonic boom loudness of the OFW is still too high for unrestricted flight overland. At this time it is unclear whether changes in the geometries will reduce the sonic boom loudness sufficiently to allow supersonic flight over land. However, due to its variable sweep the aircraft is able to cruise efficiently at boomless high subsonic Mach numbers.

Acknowledgments

This study has been supported by a Grant from the NASA Ames Research Center. The authors thank Chris Lee of NASA Ames Research Center for his cooperation.

References

[1]Lee, G. H., "Slewed Wing Supersonics," *The Aeroplane*, March 1961.

[2]Jones, R. T., "The Supersonic Flying Wing," *Aerospace America*, Oct. 1987.

[3]Van der Velden, A., "The Conceptual Design of a Mach 2.0 Oblique Flying Wing Supersonic Transport," NASA CR-1777529, May 1989.

[4]Van der Velden, A. J. M., "The Aerodynamic Design of the Oblique Flying Wing Supersonic Transport," NASA CR-177552, June 1990.

[5]Van der Velden, A., and Kroo, I., "A Numerical Method for Relating Two- and Three-Dimensional Pressure Distributions on Transonic Wings," AIAA/AHS/ASEE Aircraft Design and Operations Meeting, AIAA Paper 90-3211, Dayton, OH, Sept. 1990.

[6]Van der Velden, A., "Aerodynamic Design and Synthesis of the Oblique Flying Wing Supersonic Transport," Ph.D. Dissertation, SUDDAR 621, Stanford Univ., Stanford, CA, May 1992.

[7]Hicks, R., and Mendoza, J. P., "Oblique Wing Sonic Boom," NASA TM-X-62247, Feb. 1973.

[8]Haack, W., "Geschuss-Formen Kleinsten Wellen-Widerstandes," *Lilienthal Gesellschaft*, Bericht 139, 1941, pp. 14–28.

[9]Lomax, H., "The Wave Drag of Arbitrary Configurations in Linearized Flow as Determined by Areas and Forces in Oblique Planes," Ames Aeronautical Lab., NACA RM A55A18, 1955.

[10]Whitham, G. B., "The Flow Pattern of a Supersonic Projectile," *Communications on Pure and Applied Mathematics*, Vol. 5, 1952, pp. 301–348.

[11]Seebass, R., "Sonic Boom Theory," *Journal of Aircraft*, Vol. 6, No. 3, 1969.

[12]Carlson, H., "Correlation of Sonic-Boom Theory with Wind-Tunnel and Flight Measurements," NASA TR R-213, Dec. 1964.

[13]Carlson, H., and Maglieri, D. J., "Review of Sonic Boom Generation Theory and Prediction Method," *Journal of Acoustical Society of America*, Vol. 51, No. 2, Pt. 3, 1972, p. 675.

[14]Middleton, W. D., and Carlson, H. W., "A Numerical Method for Calculating Near-Field Sonic-Boom Pressure Signatures," NASA TN D-3082, Nov. 1965.

[15]Thomas, C. L., "Intrapolation of Sonic Boom Pressure Signatures by the Waveform Parameter Method," NASA TN D-6832, June 1972.

[16]Kane, E. J., and Palmer, T. Y., "Meteorological Aspects of the Sonic Boom," Boeing Co. System Research and Development Service Rept. RD 64-160, Sept. 1964.

[17]Pierce, A. D., and Maglieri, D. J., "Effects of Atmospheric Irregularities on Sonic Boom Propagation," *Journal of the Acoustical Society of America*, Vol. 51, No. 2, Pt. 3, 1972, p. 702.

[18]Papoulis, A., *The Fourier Integral and its Applications*, McGraw-Hill, New York, 1962.

[19]Brown, J. G., and Haglund, G. T., "Sonic Boom Loudness Study and Airplane Configuration Development," AIAA Paper 88-4467, Sept. 1988.

[20]Boeing Commercial Airplanes, "High Speed Civil Transport Study," NASA CR 4233, Sept. 1989.

[21]Von Gierke, H. E., and Nixon, W. C., "Human Response to Sonic Boom in the Laboratory and the Community," *Journal of Acoustical Society of America*, Vol. 51, No. 2, Pt. 3, 1972, p. 766.

[22]Van der Velden, A. J. M., and Kroo, I., "The Sonic Boom of an Oblique Flying Wing," AIAA 13th Aeroacoustics Conf., AIAA Paper 90-4002, Oct. 1990.